communications earth & environment

Article

A Nature Portfolio journal

https://doi.org/10.1038/s43247-026-03390-6

Sediment transport pathways and organic carbon burial impacted by offshore wind farms in shelf seas

Jiayue Chen [1], Nils Christiansen [1], Lucas Porz [1], Bo Miao [1], Mengyao Ma[1], Corinna Schrum [1,2] & Wenyan Zhang [1]

The rapid expansion of offshore wind farms increasingly impacts ocean environments. Little is known concerning synergistic effects of wind farms on large-scale sediment transport and seabed ecosystem functioning. Here, by using a three-dimensional hydro-morphodynamic model integrating wake effects, we assessed wind farm impacts on regional-scale sediment transport and organic carbon sedimentation in the North Sea. Results suggest that wind farms can alter net sediment transport fluxes by up to 30% locally, reduce mud accumulation in established depocenters and create new depocenters through long-term accumulative effects. These shifts, driven by changes in stratification and residual currents, redistribute up to 1.5 million tonnes of mud and 0.07 million tonnes of particulate organic carbon annually. Wind farms also retain ~1.5% of annual riverine sediment input to the ocean, affecting connectivity with nearshore systems like the Wadden Sea. These findings underscore the need to consider the system-wide impacts in marine spatial planning.

Wind energy plays a central role in the global transition to low-carbon energy systems. In 2023, wind power generation increased by 216 TWh, reaching over 2330 TWh globally—the second-largest growth among all renewable sources that year[1]. Offshore wind, in particular, has become a key element of national and regional energy strategies, offering high-capacity factors and substantial resource potential. In Europe, onshore and offshore wind energy supplied 19% of total electricity consumption across the EU in 2024, with especially high shares in Denmark (56%), Ireland (33%), Sweden (31%), and Germany (30%)[2].

Offshore wind farm (OWF) development is primarily concentrated in continental shelf regions such as the North Sea, Irish Sea, Baltic Sea, U.S. Atlantic shelf, and China's marginal seas (Fig. 1). These areas exhibit diverse oceanographic conditions from shallow, high-energy systems to deeper, more stratified regimes. On the other hand, they are featured by complex hydrographic characteristics shaped by tides, seafloor topography, wave climate, and freshwater inputs. These physical processes govern sediment transport, water column structure, and seabed morphology across broad spatial and temporal scales. Many of these shelf regions host mud depocenters that act as the primary sinks for terrestrially derived fine-grained sediment[3]. These depocenters play a critical ecological role as long-term carbon burial hotspots[4] and as key zones for nutrient cycling and benthic habitat functioning[5]. As such, they are particularly sensitive to anthropogenic alterations, and early studies have documented the environmental effects of OWFs in these settings[6–8]. Understanding how OWFs interact with these dynamic systems is therefore essential to managing both local and regional environmental impacts.

OWFs affect the marine environment through interactions in both the atmosphere and the ocean. Wind turbines extract kinetic energy, generating atmospheric wakes that can extend up to 70 km downstream under stable conditions, reducing wind speeds[9–11] and thereby altering Ekman transport. Wind speed reductions within wakes can exceed 40%[12], resulting in up- and down-welling velocities of several meters per day in the water column[13–15]. These vertical exchanges may affect broader-scale oceanographic properties, including currents, sea surface elevation, stratification, temperature, and salinity. Moreover, the underwater turbine foundations and piles generate turbulence and vertical mixing[16–18], producing wake zones that may enhance sediment resuspension[19]. These effects are not confined to individual turbines but can synergistically generate large-scale hydrodynamic structures in densely packed OWFs[14,15,20,21], potentially altering stratification and disrupting natural sediment transport, erosion, and deposition patterns at scales far beyond the OWFs.

Most existing studies suggest that the hydrodynamic impacts are largely confined to the immediate vicinity of the OWFs[17]. However, with the increasing number and density of installations, there is growing concern about cumulative and synergistic effects at larger spatial scales, particularly on shelf-wide stratification patterns[20–22]. A study on the impact of OWFs in

[1]Institute of Coastal Systems-Analysis and Modeling, Helmholtz-Zentrum Hereon, Geesthacht, Germany. [2]Institute of Oceanography, Center for Earth System Research and Sustainability, University of Hamburg, Hamburg, Germany. e-mail: Wenyan.Zhang@hereon.de

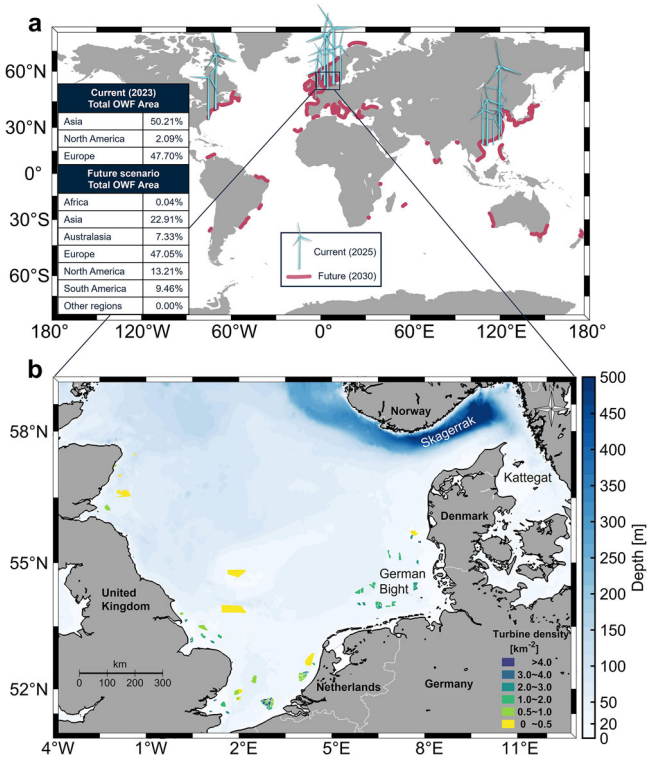

Fig. 1 | Distribution of global OWF locations. a The blue turbines represent the present-day situation (operating and under construction) in 2023. The red lines represent the near-future projection till 2030 (operating, under-construction and early planning). The table shows percentage distribution of OWF area across the regions. Data on OWF locations, names, and areas were obtained from the 4C global offshore database version of May 2025 (obtained via https://map.4coffshore.com/offshorewind/). **b** Distribution and turbine density of existing OWFs in the North Sea. The country borders were obtained from the Natural Earth Admin 0 version 5.11 (obtained via https://www.naturalearthdata.com/downloads/10m-cultural-vectors/10m-admin-0-countries/).

the North Sea revealed the emergence of basin-scale oceanographic structures, including shifts in currents, sea surface elevation, and stratification[20,21]. While some regional modeling studies estimate that OWF-induced changes in hydrodynamic conditions can reach up to 10% in magnitude[20,22,23], the broader implications for long-term sediment fluxes, erosion and deposition patterns, organic carbon burial and sediment connectivity between offshore and nearshore coastal systems remain poorly quantified, especially under scenarios of large-scale OWF deployment.

In this study, we developed a three-dimensional hydro-morphodynamic modeling framework to investigate the effects of OWFs on regional-scale sediment transport and sedimentation of organic carbon. The exemplary model application area is the North Sea—a key area for developing offshore wind energy as part of Europe's green transition. Our simulations incorporate parameterizations of both atmospheric wake effects and oceanic turbulence mixing induced by OWFs structures. We focus mainly on the physical effects of OWFs. Potential biological effects induced by turbine-colonizing fauna (e.g., filter feeders such as blue mussel) are not included in our modeling. Rather than focusing solely on local changes near turbine arrays, our study explores broader system responses, including shifts in residual sediment fluxes and changes to established depositional patterns. The results highlight how OWFs can modify fine-grained sediment including particulate organic carbon distribution on the surface of the seabed and affect connectivity between offshore and coastal environments. These insights contribute to a deeper understanding of OWFs' role in reshaping seabed morphology and sedimentary carbon stock and underscore the importance of incorporating sediment dynamics into marine spatial planning and ecosystem management strategies.

Results and discussion

Sedimentation of mud and organic carbon modified by OWFs

The broad North Sea shelf is generally featured by energetic tidal currents, waves and winds, with deposition of fine-grained sediment (sediment grain diameter <0.063 mm; Fig. 2b), namely mud, mainly confined in several disconnected depocenters (Fig. 2a). Surface seabed particulate organic carbon (POC) content is strongly correlated with mud content ($r = 0.66$, $P < 0.001$)[4,24], suggesting a high similarity of their transport and deposition dynamics (Fig. 2b). Most existing OWFs in the North Sea are located on the sandy seabed in the shallow southern part (Fig. 1b), with a few near a primary mud depocenter, namely the Helgoland Mud Area (HMA), in the southeastern coastal area, the German Bight.

To assess the changes in transport and sedimentation of mud and POC driven by OWFs, we conducted 15 numerical experiments (see Methods & Table 1). These experiments were used to assess the uncertainty caused by assumptions or empirical parameterizations in the model regarding sediment and POC properties. Two key parameters determining mobilization and sedimentation of mud and POC, namely particle settling velocity and critical shear stress for resuspension, are considered to vary within a certain range. We calculated the ensemble mean and standard deviation of the simulation results in which OWF impacts are included and compared these to their respective reference simulations excluding OWF impact (Table 1). Model results for two consecutive years, namely 2013 and 2014, are analyzed. These years were selected because they represent contrasting conditions of river discharge, with high values in 2013 and low values in 2014 (Supplementary Fig. 1), thereby allowing the simulations to capture system responses to distinct riverine input conditions. OWF effects in hydrodynamics (e.g., current velocity, stratification and mixing) have been validated in our earlier modeling studies[20,25]. Modeled sediment dynamics, namely suspended sediment concentration above mud depocenters and the large-scale sediment transport patterns, have been validated against observations by Chen et al.[26]. In this study, we thus focus on assessment of OWF-induced changes in large-scale sedimentation patterns.

In this study, remobilization is defined as the net in-situ resuspension of sediment and POC driven merely by OWF-induced changes in bottom shear stress. The term redistribution denotes the combined gross effect of OWFs in (i) remobilization of in-situ surface sediments and POC, (ii) long-distance transport and repeated deposition-resuspension cycles of allochthonous mud imported from the open Atlantic Ocean and through the English Channel, and (iii) riverine sediments and POC that enter the regional resuspension–deposition cycles in the North Sea. The net budget represents the overall balance of erosion and deposition over the 2-year simulation period, i.e., the final gain or loss of sediment and POC on the seabed.

The simulated multi-year sediment mass changes in surface seabed due to OWFs reflect potential longer-term sediment responses. Natural sedimentation rates in the North Sea (excluding the Kattegat) are estimated at the magnitude of 13–23.5 Mt yr^{-1} (e.g., Eisma[27]). Against this background, our results show that OWFs induce an annual mean redistribution of 1.1 ± 0.3 Mt yr^{-1} of mud on the North Sea continental shelf. Despite this substantial gross redistribution, the resulting net sediment budget change is small ($4.2 \times 10^{-2} \pm 7.8 \times 10^{-2}$ Mt yr^{-1}; Fig. 2c). The redistribution also leads to modifications in surface seabed sediment composition, corresponding to an approximate 0.1% average change in mud fraction of the surface 10 cm sediments on an annual basis, with local maximum up to 1% (Supplementary Fig. 2). Transport and deposition of POC are closely related to mud[4,24]. As a result, changes in POC content in surface sediment show a strong correlation with changes in mud content. Across the entire North Sea shelf, the annual mean redistribution of POC mass caused by OWFs is $4.5 \times 10^{-2} \pm 1.4 \times 10^{-2}$ Mt C yr^{-1} (Fig. 2d) with a net gain ranging from 2×10^{-4} to 1.1×10^{-2} Mt C yr^{-1}.

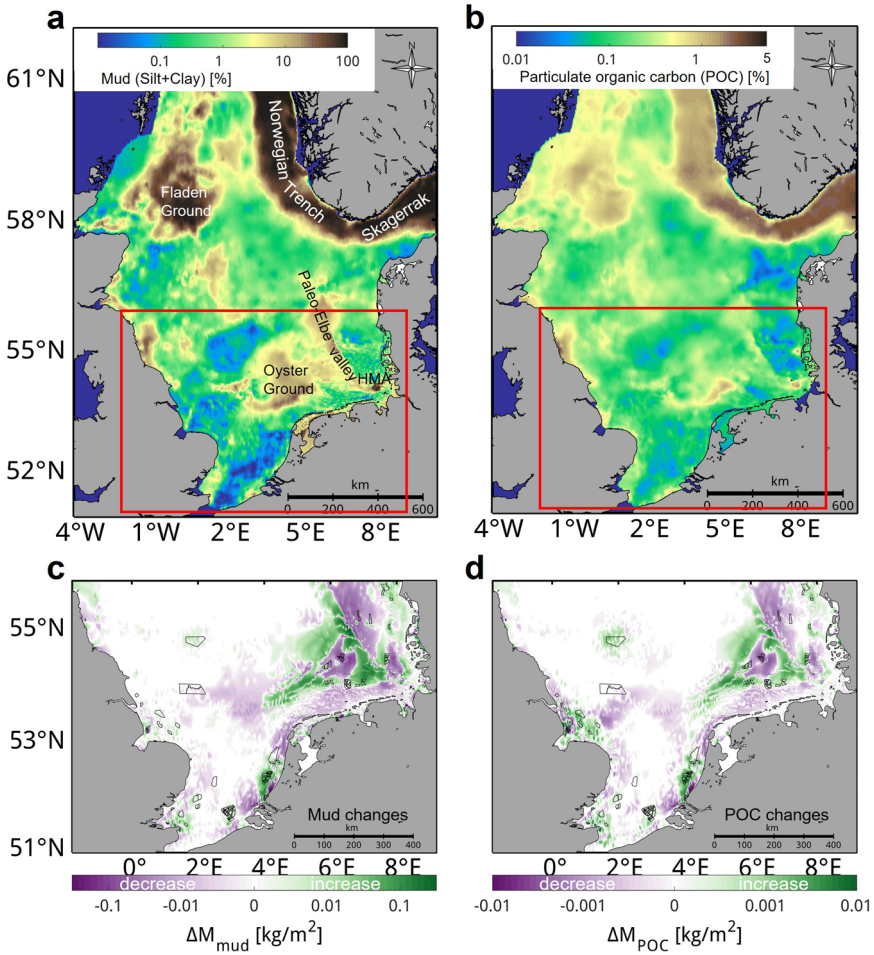

Fig. 2 | Distribution of mud and particulate organic carbon in the North Sea surface sediments and simulated changes caused by offshore wind farms. a Mean mud content (%) in the upper 10 cm sediment. **b** Mean particulate organic carbon content (%) in the upper 10 cm sediment. Sediment data in panels (**a**) and (**b**) are compiled from the datasets listed in Supplementary Table 1. **c** Annual mean change of mud mass (ΔM_{mud}) calculated by the difference in the simulation results between the experiments of OWF impact and respective reference simulations. **d** Similar to (**c**) but for POC mass (ΔM_{POC}). Positive and negative values in (**c**) and (**d**) refer to increase and reduction in mass, respectively. The black polygons in (**c**) and (**d**) represent the locations of OWFs.

Table 1 | Annual mean changes of mud and POC in the North Sea and German Bight

Experiments	ΔM_{mud} [k ton/year]		ΔM_{POC} [k ton/year]	
	North Sea	German Bight	North Sea	German Bight
S1	1010.8 (29.1)	548.4 (101.7)	39.2 (1.5)	15.9 (2.4)
S2	1462.5 (42.9)	694.5 (193.1)	63.8 (3.4)	22.2 (5.4)
S3	1195.9 (−2.0)	665.9 (65.4)	46.8 (1.3)	19.4 (1.6)
S4	1036.8 (−2.2)	620.6 (59.2)	39.0 (2.5)	17.8 (2.4)
S5	1224.7 (−8.8)	718.7 (126.4)	47.5 (0.2)	21.3 (5.6)
S6	1257.0 (216.1)	519.5 (209.6)	58.2 (11.4)	18.1 (8.3)
S7	534.3 (3.4)	292.9 (19.0)	22.1 (0.3)	8.4 (0.3)
Mean	1103.1 ± 292.3 (42.3 ± 78.5)	580.1 ± 146.3 (110.6 ± 70.7)	45.2 ± 13.7 (2.9 ± 3.9)	17.6 ± 4.6 (3.7 ± 2.8)

These results are derived from our calculation of mass differences between each windfarm experiment and respective reference experiment based on simulation of 2 years (2013–2014). The amount of redistribution is shown in numbers and the net budget change is indicated in parentheses.

At the regional scale, the total annual riverine input to the North Sea contains ~10 Mt of mud and 0.4 Mt of POC[28], with a major portion being transported across the broad shelf and ultimately deposited in the mud depocenter in Skagerrak and Norwegian Trench[27,29]. Our simulations suggest that OWFs retain ~1.5×10^{-1} Mt yr^{-1} of riverine sediment and 6×10^{-3} Mt C yr^{-1} of POC, corresponding to ~1.5% of the annual offshore riverine discharge to the North Sea. Given that the annual net sedimentation of POC in the North Sea is ~1 Mt C yr^{-1} according to Diesing et al.[30], OWFs notably influence the sedimentation of POC and additionally lead to ~1% increase of annual net POC sedimentation on the North Sea shelf.

It is worth noting that wave-induced effects (e.g., enhanced resuspension and mixing) account for ~13–35% of the total OWF-induced changes in mud and POC redistribution. However, waves do not alter the direction or spatial structure of the OWF-induced transport pathways (Supplementary Fig. 3). This suggests that tides and wind-driven circulation are the main driving forcing for large-scale transport pathways.

Sediment redistribution caused by OWFs is particularly pronounced in the German Bight, which hosts the primary mud depocenter, the Helgoland Mud Area (Fig. 2a). In the German Bight, the annual mean redistributed mud mass among the experiments ranges from 2.9×10^{-1} to 7.2×10^{-1} Mt yr^{-1}, resulting in a net gain of 1.9×10^{-2} to 2.1×10^{-1}Mt yr^{-1}. In this region, the net accumulated mass is equal to ~10% of the total redistributed mass on the entire North Sea shelf, suggesting that the southern North Sea especially the German Bight is a sink of OWF-induced redistributed mud. Net mud gain can locally reach up to 508 g m^{-2} yr^{-1} (~0.6 mm in sediment thickness) within the Paleo-Elbe valley and Oyster Ground (Fig. 2c). The change of sedimentary POC mass in the German Bight reflects this spatial pattern: 8.4×10^{-3} to 2.2×10^{-2} Mt C yr^{-1} of POC is redistributed with a net change of $3.7 \times 10^{-3} \pm 2.8 \times 10^{-3}$ Mt C yr^{-1} in surface sediment.

Our results suggest that the mud accumulation decreases in the primary depocenter (HMA) in the order of 5×10^{-5} to 2.7×10^{-4} Mt yr^{-1} (Supplementary Fig. 4) but increases in other muddy sites (Paleo-Elbe valley and Oyster Ground) under the large-scale, long-term influence of OWFs. The decreased accumulation on the primary depocenter in the HMA is due to a reduced depositional rate rather than an enhanced erosion (Supplementary Fig. 4). Overall, ~52% of total sediment redistribution caused by

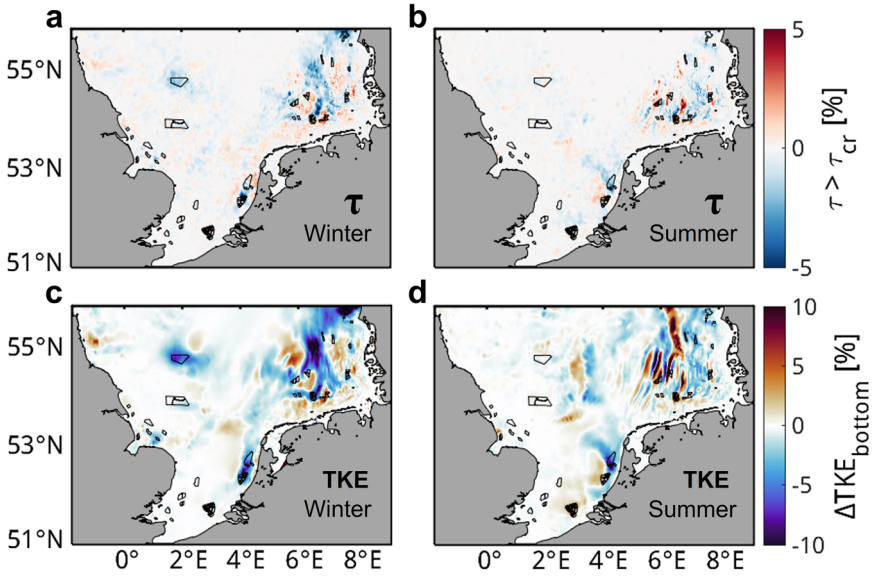

Fig. 3 | Seasonal response in bottom shear stress and bottom turbulent kinetic energy due to offshore wind farm effects. a, **b** Estimated relative changes in the duration of bottom shear stress (τ) exceeding 0.1 Pa defined as the critical value for resuspension of mud (τ_{cr}) in boreal winter (December–February) and summer (June–August) months, respectively. Positive and negative values indicate enhanced and reduced bottom shear stress caused by OWFs compared to the reference simulation excluding OWFs, respectively. **c**, **d** Similar to a and b but for turbulent kinetic energy (Δ TKE_{bottom}) in the bottom water. The locations of offshore wind farms are shown by black polygons.

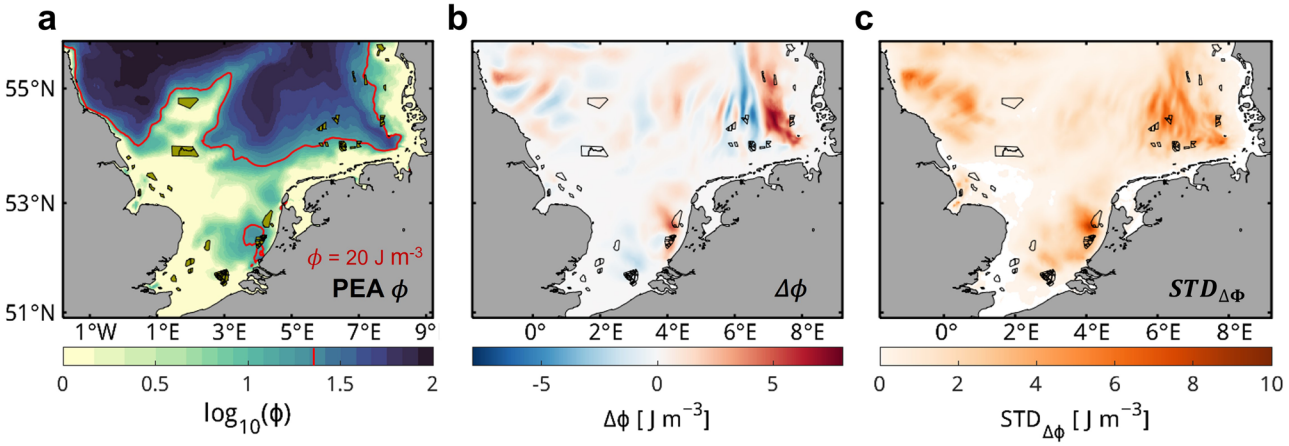

Fig. 4 | Seasonal response of potential energy anomaly PEA (Φ) and standard deviation (STD$\Delta\phi$) of its change to atmospheric and hydrodynamic changes caused by offshore wind farms. a Mean PEA calculated in the reference simulation for summer season (June–August). The red line indicates the threshold of stratification ($\Phi = 20$ J/m^3), which can indicate the position of the tidal mixing front in the German Bight[26]. **b** Estimated relative changes of the PEA in summer caused by OWFs. Positive and negative values indicate increased and decreased PEA by OWFs, respectively. The locations of offshore wind farms are shown by black polygons. **c** Similar to (**b**) but for the standard deviation ($STD_{\Delta\phi}$) of the change in PEA.

OWFs on the North Sea shelf occurs in the German Bight, highlighting its sensitivity to OWF-induced changes in sediment dynamics.

Process-based understanding of OWF impacts

Fine-grained sediment dynamics in shelf seas are controlled by complex environmental conditions that influence the formation and maintenance of mud depocenters. These dynamics can be disrupted by the presence of OWFs. Reduced and increased bottom current strength promotes deposition and erosion of mud, respectively. Depositional or erosional environment can be identified using indicators, such as bottom shear stress that is closely related to turbulent kinetic energy in the bottom layer[31]. Sediment resuspension typically occurs when bottom shear stress exceeds a certain threshold[32] (e.g., 0.06 Pa for unconsolidated silts and 0.1 Pa for very fine sands). To identify and characterize excess resuspension caused by OWFs, we calculated the changes in the duration during which the threshold of resuspension for coarse silts and very fine sands, as dominant sediment types in the depocenters, is exceeded. Our results show that enhanced bottom shear stress and turbulent kinetic energy (TKE; Fig. 3), especially downstream of OWFs following the mean currents, increase the frequency and intensity of sediment resuspension. In contrast, reduced bottom shear stress in muddy areas such as the Paleo-Elbe valley and Oyster Ground favors sediment deposition. The change in the magnitude shows seasonal variability, with more extensive and larger changes during winter when higher wind speeds amplify the effects of wind speed reductions caused by OWFs and larger additional turbulence drag and mixing caused by wind farm infrastructures. It is noteworthy that changes in the winds caused by OWFs are most responsible for the large-scale changes beyond the location of OWFs, since hydrodynamic drag and enhanced TKE in water due to wind turbines are mainly confined within OWFs with a limited spatial extension (within a few km) to the downstream side (Supplementary Fig. 5).

Changes in the atmospheric conditions caused by OWFs can influence large-scale oceanic circulation, thereby altering the intensity and distribution of stratification[20–22]. To assess this effect, we calculated the potential energy anomaly (PEA, see Methods) and its standard deviation as proxies for stratification strength and stability (Fig. 4). PEA provides a quantitative measure of stratification: higher PEA values indicate that more mechanical energy is required to homogenize the water column and thus correspond to stronger density stratification. Our results indicate that OWFs lead to an

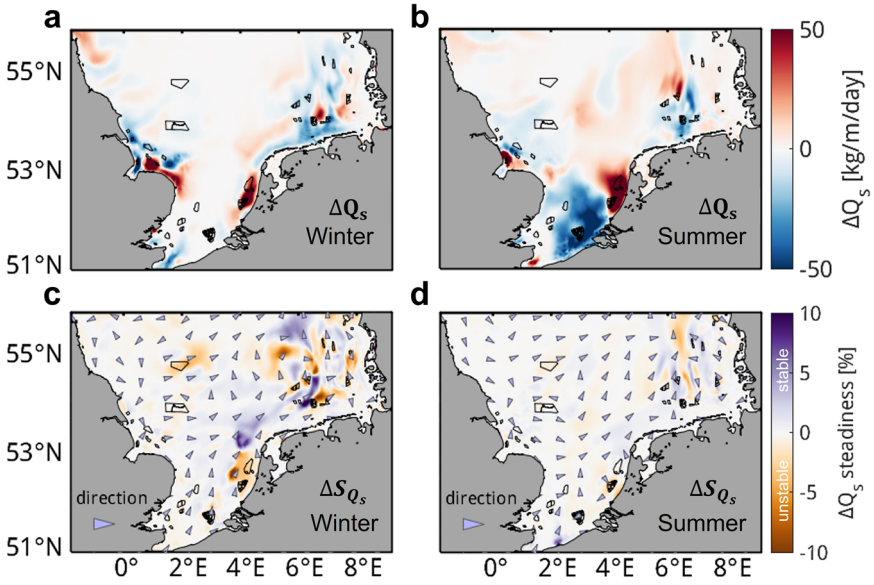

Fig. 5 | Seasonal response of depth-integrated residual sediment flux (Q_s) and transport direction steadiness to atmospheric and hydrodynamic changes caused by offshore wind farms. a Mean change of Q_s in winter (December–February). Positive and negative values indicate increase and decrease of Q_s caused by OWFs, respectively. **b** Similar to a but for summer (June–August) months. **c** Mean change of the steadiness of transport direction in winter (December–February, see Eq. (7) in Methods for definition). Positive and negative values indicate increase and decrease of steadiness caused by OWFs, respectively. **d** Similar to (**c**) but for summer (June–August) months. The arrows in (**c**) and (**d**) indicate the seasonal averaged direction of Q_s derived from the reference simulation.

overall increase of stratification within areas surrounded by OWFs, such as the Paleo-Elbe valley, thereby promoting sediment accumulation. This is because the local mixing enhancement by turbines is outweighed by the broader reduction in wind-driven turbulence caused by wind deficits, leading to an overall net increase in stratification downstream of the OWFs. This enhancement of stratification is most pronounced and stable in the eastern German Bight, while in the western part, stratification tends to weaken and exhibits greater variability (Fig. 4c). Despite these changes, the spatial location of the salinity and tidal mixing fronts remains largely unchanged under OWF influence (Supplementary Fig. 6). On the other hand, intensification of tidal mixing front is shown by an increase in the PEA gradient across the fronts (Fig. 4b), suggesting localized changes in mixing dynamics (Fig. 4b).

Notably, the synergistic influence of multiple OWFs appears to amplify these changes in hydrodynamics. The combined atmospheric wake effects and enhanced oceanic turbulence from clustered installations create feedback that modify stratification patterns and mixing processes across a broader area[20] (Figs. 3 and 4). These synergistic effects are particularly remarkable in the German Bight, where they shape sediment and POC transport, resuspension, and burial of sediments and POC at the regional scale (Fig. 2).

The major mechanism for formation of mud depocenters in high-energy coastal environment is sediment trapping and deposition caused by density fronts associated with freshwater plume[33], thermohaline[34,35], tidal mixing and/or downwelling[36,37]. On the primary mud depocenter in the Helgoland Mud Area, the general spatial structure of the density fronts and the associated sediment convergence and trapping mechanisms remain relatively stable[26]. The tidal mixing front, which is established in summer and diminishes in winter, is found to limit sediment deposition on the seaward side of the mud depocenter in HMA. Consequently, the offshore extension of HMA is restricted[26]. OWF-induced changes in hydrodynamics lead to further enhanced resuspension near the tidal mixing front, primarily through an enhancement of the density gradient that results in intensified frontal circulation[26] (Supplementary Fig. 4). In contrast, the impact of OWFs on the salinity front is minimal in the German Bight, as most OWFs are located further offshore, beyond the direct reach of the freshwater plume. OWF-induced changes mainly occur at the tidal-mixing front and its offshore, modifying transport and depositional flux of sediment and POC there, leading to reduced deposition in the primary depocenter (HMA) and enhanced deposition in secondary mud deposits (Paleo-Elbe valley and Oyster Ground) near the HMA (Fig. 2b).

Our results suggest that changes in the residual sediment transport flux, calculated by averaging sediment transport flux at each time step (2 min) over each season, exhibit strong seasonal variability and extend beyond the immediate vicinity of OWFs, exerting a regional-scale influence. During the winter season, most changes are concentrated in the nearshore of the southern North Sea (Fig. 5a), along the established sediment transport pathways (Fig. 5c & Supplementary Fig. 7). In summer, changes are more spatially extended, particularly along the southern Dutch coast, where a considerably decrease in sediment flux occurs near the estuaries, accompanied by an increase further north in the OWF cluster region (Fig. 5b). The seasonal response of residual sediment transport flux in this area is closely linked to stratification associated with the freshwater plume. In winter, when stratification associated with the temperature gradient is minimal, the water column is locally stratified due to river discharge despite strong wind forcing, and OWF-induced hydrodynamic changes produce only local effects on sediment resuspension and transport that are mainly restricted in the OWF area. By contrast, in summer, extensive stratification driven by river discharge, temperature gradients, and reduced wind forcing increases the sensitivity of the system to OWF-induced mixing (Supplementary Fig. 8). Here, OWFs increase mixing near the estuaries (Fig. 4b), causing a local reduction in the horizontal transport flux. Meanwhile, the enhanced stratification further north in the OWF cluster (Fig. 4b) amplifies downstream transport flux. This effect is particularly pronounced in summers (e.g., 2013) featured by higher river discharge reinforcing stratification, whereas low river discharge in summer such as that in 2014 produces a milder response (Supplementary Fig. 9). The Rhine estuary in the southern Dutch coast provides a major freshwater input to the region[38]. The river plume is mainly driven by the coastal current that is directed northeastward. In the downstream of the Rhine outflow, a consistent OWF-induced increase in residual sediment flux occurs during both winter and summer. The presence of OWFs in this area leads to reduced turbulent mixing in the water column (Fig. 3) and enhanced stratification (Fig. 4b). As a result, mud primarily delivered by the Rhine outflow accumulates around the wind farm structures (Fig. 2). This reduces alongshore sediment transport toward the German Bight, thereby limiting the supply to the primary depocenter in the Helgoland Mud Area. Different from the Dutch coastal water, the parts of the German Bight where OWF clusters are located are less influenced by freshwater plumes. At a seasonal scale, these modifications show that OWFs can alter net sediment transport fluxes locally by up to 30% (Supplementary Fig. 7).

OWFs influence not only the magnitude of sediment transport flux but also the transport direction (Fig. 5c, d). While the residual sediment

transport generally follows the residual current directions (Supplementary Fig. 10), the presence of OWFs and their associated modifications in hydrodynamics introduce variations in the transport direction. Such variation is featured by decreased steadiness in the OWF area and their downstream side, with patches of increased steadiness nearby (Fig. 5c, d). These variations are most prominent in winter and weakest in summer, in contrast to the seasonal patterns of the magnitude of transport flux. This higher variability of transport direction in winter is mainly due to a larger variability of wind in stormy winter[26].

Implications for sediment transport and OC burial in global shelf seas

Our findings from the North Sea show that the influence of OWFs extends far beyond localized changes near individual turbines, reshaping sediment and POC transport and deposition patterns across wider shelf regions. The disruption of sediment fluxes and redistribution in the established mud depocenter (Helgoland Mud Area) demonstrates that OWFs can influence the long-term stability of mud depocenters and their ecosystem functioning, such as carbon storage. Sediment exchange between the North Sea and the world's largest intertidal system, the Wadden Sea, may also be affected by continuing expansion of OWFs in the German Bight. Such changes could affect the long-term maintenance of the Wadden Sea system, which relies on sufficient sediment supply to keep pace with ongoing and future sea-level rise[39,40]. Although the modeled surface mud and POC content changes are relatively small- corresponding to less than 1% per year- the relatively consistent change over multiple years suggests that the effect may accumulate over several decades and lead to noticeable degradation of existing depocenters and formation of new ones. Moreover, the continued expansion of OWFs is likely to amplify these effects[21], further influencing sediment stability and redistribution across continental shelves.

These results hold broader relevance given the expanding footprint of OWFs in shelf seas globally (Fig. 1a), as such impacts are not unique to the North Sea. Formation of mud depocenters across continental shelves is governed by similar sediment trapping and deposition mechanisms associated with frontal systems, such as those reported on the Amazon shelf, Bay of Biscay, East China Sea, and Iberian shelf[33,34,37,41]. Many of these regions are also part of OWF development plans (Fig. 1a). Our findings suggest that OWFs, through persistent alterations in currents and water column stratification, have the potential to modify regional-scale sediment transport pathways, gradually and accumulatively affecting sediment budgets, seabed morphology, and benthic ecosystems over decadal timescales.

In parallel, changes in sediment transport affect the distribution and burial of POC. Altered deposition patterns and enhanced resuspension in OWFs may reduce carbon sequestration in existing burial hotspots such as established mud depocenters. Meanwhile, they could increase lateral POC transport fluxes to other parts of the shelf. These shifts in carbon dynamics highlight the need to consider biogeochemical impacts alongside physical changes when assessing the broader environmental footprint of OWFs. Several recent modeling studies further support this complexity. For example, Daewel et al.[22] emphasized the biogeochemical consequences of OWFs, showing up to 10% local increase in sedimentary organic carbon after one year due to enhanced primary production, though the overall increase of POC in surface sediment across the entire North Sea remains modest at 0.2% according to their simulations. Ivanov et al.[42] investigated the role of epifauna and found that mussel-induced bio-deposition on turbine foundations considerably enhanced organic carbon sequestration, with total organic carbon deposition increased by up to 50% within 5 km of monopiles and detectable effects extending as far as 30 km along the main residual current. De Borger et al.[43] further demonstrated that enhanced sedimentation due to fecal pellets expelled by filtering epifauna within OWFs can substantially increase reactive organic carbon burial. Their estimates show a local increase of mineralization rates by 26.8–29.5% and organic carbon stocks in the upper 10 cm of sediment by 10-11% in present-day and future situations after 20 years of the installation of OWFs. When integrated over the Belgian Part of the North Sea, however, the corresponding increase is only 0.2–0.5%, highlighting the strong contrast between local and regional OWF impacts.

Besides direct physical remobilization and biogeochemical influence in primary production, OWFs also impact sedimentary carbon stock in other aspects. Heinatz and Scheffold[44] examined how offshore wind farms influence organic carbon stocks throughout their life cycle, including losses from seabed disturbance during construction and decommissioning, and gains from artificial reef effects during operation. They estimated a net increase of ~0.05 Mt yr^{-1} in sediment organic carbon stock in OWF areas of the southern North Sea, considering both commissioned and planned OWFs for future. This positive value largely reflects enhanced carbon retention and biological production around turbine foundations, which outweigh the initial release of carbon during turbine installation. The estimated net increase is roughly 8 times greater than the amount of POC retention from riverine discharge reported in our study caused by operating OWFs, since their estimate includes also the OWFs that are planned but not yet in operation whereas our estimates focus only on the physical transport and sedimentation effects associated with currently operating wind farms. These findings are not contradictory but rather complementary to address the complexity in quantifying OWF impact on carbon cycling and sequestration. Our study contributes to this effort by focusing on modifications in large-scale transport and deposition processes. Together, these findings underscore that carbon dynamics around OWFs are shaped by a complex interplay of physical, ecological, and operational factors. Shelf seas with OWFs therefore cannot be characterized by a simple increase or decrease in carbon storage. Instead, they are driven by a complex set of processes that require integrated, multidisciplinary assessment.

While our study represents, to the best of our knowledge, the first quantitative assessment of OWF impact on regional scale sediment transport and deposition patterns based on state-of-the art parameterization schemes combining both atmospheric and ocean compartments, some model limitations are worthy of noting. In particular, small-scale processes such as Kármán vortices[45] and local upwelling/downwelling downstream of wind turbines[14], which could contribute to localized seabed scouring, are not fully resolved in our coastal ocean model with grid size from several hundred meters to several kilometers. Previous numerical studies have shown that wind-wake effects can generate localized upwelling/downwelling dipoles in stratified waters, with vertical velocities exceeding 1 m day^{-1} and spatial footprints extending several kilometers around wind turbines[13,14]. These features can alter stratification and mixed-layer depth[15], potentially enhancing primary production at meso- to submesoscale (horizontal scale of 1–40 km) when wind directions remain stable for at least ~8–10 h with moderate speeds[13]. While these small-scale processes may contribute to localized seabed scouring, organic carbon cycling, and short-lived pulses of productivity, parameterization of their effect in a form of enhanced turbulence mixing like the one used in our model is able to capture a larger-scale ecosystem response to some extent[22]. On the other hand, resolving individual turbine foundations at meter-scale grid resolution (e.g., Hosseini et al.[46]) is computationally demanding and not feasible for long-term, regional-to-global scale simulations addressing sediment and carbon budgets. Therefore, process-based parameterizations representing integrated effect of multiple turbines in OWFs remain necessary to ensure physically meaningful and computationally tractable simulations to assess cumulative, basin-scale impacts over multi-year timescales. Existing field-based measurements are only able to indicate local seabed changes (e.g., scour around the piles) but not sufficient to validate the large-scale subtle OWF-induced seabed changes simulated by our model, which are less than 1 mm per year (maximum OWF-induced deposition averaged over a 1 × 1 km grid cell is ~0.6 mm/yr). Robust near-term detection is most feasible in the atmospheric wake field (Supplementary Table 2) and in spatially resolved ocean measurements specifically designed to resolve wake-scale structures in surface currents, waves and turbidity. Long-term, continuous observations are required to capture large-scale seabed effects, which would accumulate and become detectable only after a few decades to provide robust field validation. Further, uncertainties related to parameterizations and

numerical implementation of biological factors, such as epifauna inhabiting on turbine foundations and their impact on the hydrodynamic drag and carbon flows, present a need for further research.

In conclusion, our findings point to a potential long-term redistribution of mud and POC driven by OWF-induced changes in hydrodynamics and stratification. These processes may reshape seabed morphology and affect the stability of coastal and offshore sedimentary systems such as mud depocenters and their ecosystem functioning. Incorporating these insights into marine spatial planning and coastal management strategies is essential to ensure a sustainable development of offshore wind energy.

Methods

Model configuration

We employed a coupled hydro-morphodynamic model that integrates the three-dimensional Semi-implicit Cross-scale Hydroscience Integrated System Model (SCHISM)[47] with the sediment transport and morphodynamics model (MORSELFE)[48] and the wave model (WWMIII)[49]. The wave model is implemented within the SCHISM framework, enabling two-way wave–current interactions and joint effects on sediment dynamics.

The configuration used in this study is based on model setups presented in earlier studies by Kossack et al.[50] and Porz et al.[28], and has been further refined and validated for nearshore sediment dynamics by Chen et al.[26]. In addition, the simulated wave properties (significant wave height, wave period and direction) show satisfactory agreement with observation (Supplementary Fig. 11). The model domain covers the entire north Atlantic Ocean including the North Sea and the Baltic Sea with two open boundaries at north and southwest of the North Sea. The unstructured triangular grid in the horizontal dimension has the resolution up to ~1 km in the OWFs and adjacent areas to capture key mesoscale and submesoscale features such as the internal baroclinic radius of the deformation (~10 km in the North Sea), thereby better reproduce the impacts of the OWF wind wakes[14,51]. The vertical dimension adopts the Localized Sigma Coordinates with Shaved Cells (LSC^2) to resolve the near-bottom dynamics with a maximum of 52 layers. Bathymetric data were interpolated from the 50×50 m resolution dataset provided by the European Marine Observation and Data Network (EMODnet). A full list of observation datasets as well as the purpose of these datasets for our study are provided in Supplementary Table 1.

The model simulations were conducted using realistic atmospheric forcing, open boundary forcing and river discharge from 2012 to 2014, including a one-year spin-up under the initial setting to ensure model stability. In numerical experiments involving OWFs, an additional one-month spin-up has also been conducted to allow adaptation of ocean circulation to the impact of OWFs. The results for 2013 and 2014 were analyzed. The reason for extrapolating the results for 2013 and 2014 to a longer time scale is that these two years represent contrasting conditions of river discharge, with high values in 2013 and low values in 2014 (Supplementary Fig. 1). This allows the simulations to capture system response to distinct riverine input conditions along the coast. A general consistency in the residual transport patterns with existing regional-scale modeling studies from earlier years has been shown in our earlier study[26].

Seabed sediment properties and organic carbon content

The surface seabed sediment configuration is based on that from Chen et al.[26] with further refinement in nearshore area by integrating high-resolution local datasets. We specified initial sediment mud content in the North Sea using interpolated measured data provided by Bockelmann et al.[52], together with sediment grain size data from the EasyGSH-DB data products[53]. To better resolve the German Bight and Wadden Sea, these datasets were complemented with additional sediment information from the SIBES[54] and AufMod[55] projects. The spatial distribution of surface POC was initialized using the interpolated measured data from Bockelmann et al.[52], provided at 3×3 km resolution and covering the entire North Sea. In the sediment module, POC is treated as a conservative tracer. POC deposited in the surface sediment layer is assumed to be recalcitrant and does not undergo benthic remineralization. This setting is based on the results of Zhang et al.[4] showing that labile OC in surface sediments of the North Sea shelf is largely depleted in stormy winter and only refractory/recalcitrant POC can sustain repetitive cycles of resuspension–transport–deposition in such a high-energy shelf sea. As a result, the model captures physical transport and sedimentation processes but does not explicitly represent biogeochemical degradation of POC in the seabed. Daily river forcing includes river discharge and sediment loads from over 100 major rivers within the model domain. A constant concentration of 40 mg L^{-1} for discharged sediment is specified at the Elbe river boundary according to the median value derived from nine major rivers in the southern North Sea by Abril et al.[56]. An overview of the sediment and POC datasets is provided in Supplementary Table 2.

Two key parameters, namely particle settling velocity (w_s) and critical shear stress for resuspension (τ_c), largely determine mobilization and sedimentation of mud and POC. To estimate the sensitivity of simulated transport, erosion and deposition patterns to variation of these two parameters, we designed a set of simulations adopting different values of w_s and τ_c that are within reported range from existing literature.

Numerical implementation of offshore wind farms effects

The impact of OWFs is implemented through two parameterizations, one for atmospheric (wind) wakes behind wind turbine clusters and one for subgrid oceanic wakes downstream of turbine clusters.

The wind wakes are represented by a top-down wake parameterization that describes wind speed deficits on the downwind side of offshore wind farms[20]. The wind speed deficits are calculated by

$$u(x,y) = u_0\left(1 - \Delta u(x,y)\right), \tag{1}$$

$$\Delta u(x,y) = \alpha e^{-x/\sigma - (y/\gamma)^2}, \tag{2}$$

where u is the wind speed on the downwind side of windfarm, x and y are the horizontal distance along the downwind axis and from the central wake axis respectively, α is the maximum relative deficit, σ is the exponential decay constant, u_0 is the undisturbed wind field, Δu is the wind speed deficit and $\gamma = L/3$ is an exponential decay constant where L is the wind farm width. At each time step, according to the prevailing wind direction, $\Delta u(x, y)$ is evaluated at every surface grid node in a wind-aligned coordinate system and applied directly to the local wind vector, yielding a spatially varying two-dimensional wind speed deficit field. In the wake parameterization, the coordinate origin is set at the lee side of each wind farm to describe the wind speed deficits and wake recovery, so that Δu represents the combined wake effect of the entire farm rather than individual turbines. Individual turbine contributions are integrated through the overall wake width and the maximum deficit parameter α. α is also used to define the relative wind speed deficit within the OWFs. The reported ranges of α is 5–10% and σ is 5–70 km based on existing studies (Supplementary Table 2). In reality, α and σ vary with wind farm layout, turbine drag, turbine density, and atmospheric conditions including wind field characteristics, stability, vertical momentum fluxes. Because no universal empirical formulation exists to capture these dependencies, we adopted representative mean values supported by measurements and Synthetic Aperture Radar (SAR)-based statistics, and used $\alpha = 10\%$ and $\sigma = 30$ km for the North Sea OWFs, These values are consistent with previous modeling[20–22] and observations (Supplementary Table 2) of wake deficits and lengths at the sea surface. The atmospheric wake parameterization modifies the wind field at every time step and includes operational constraints, applying wake effects only when wind speeds at hub height range between 3 and 25 m s^{-1}.

To account for oceanic wakes, a hydrodynamic drag caused by the monopiles and enhanced turbulence kinetic energy (TKE) downstream of turbine clusters are added to the hydrodynamic equations.

We follow the method of Christiansen et al.[21,23], where a drag parameterization was added to the hydrostatic momentum equation and enhanced turbulent kinetic energy and dissipation were added to the turbulence closure scheme. The additional drag force per unit mass is computed as

$$\vec{G}_d = -\frac{1}{2} C_d N \frac{d}{A} |\vec{u}| \vec{u}, \tag{3}$$

where C_d is the drag coefficient, N is the number of monopiles within each grid cell, d is the diameter of the monopile cylinder, A is the horizontal area of the grid cell containing the cylinders, and $\vec{u}$ is the velocity of the free stream velocity vector[16,57]. The arrows over $\vec{G}_d$ and $\vec{u}$ denote vector quantities, which act in opposite directions as determined by the governing function. In this study, we adopted a uniform diameter of the monopile cylinder $d = 8$ m and the number of monopiles at each grid cell were calculated based on the observation data of offshore wind turbines from 4C Offshore (https://map.4coffshore.com/offshorewind/).

Representative values of the turbine drag coefficient (C_d) were adopted from our earlier study in Christiansen et al.[21,23]. In that study, a thorough sensitivity analysis across a possible range of values was performed. The drag effect is strongly dependent on the choice of scaling parameters, particularly the turbine diameter (d) and drag coefficient (C_d), of which C_d exerts the largest uncertainty. Experimental studies for cylinders with different foundation structures in unstratified flows suggest C_d values between 0.2 and 1.3 (e.g., Shih et al.[58]; Sumer[59]; Carpenter et al.[16]), depending on turbulence intensity, surface roughness, and local flow conditions. According to Christiansen et al.[21,23], a value of $C_d = 0.63$ corresponds to moderate mixing effect at a large-scale beyond the wind farms. In this study, we adopted a higher value $C_d = 1$ to compensate the mixing effect at a coarser grid resolution so that the simulated mixing effect is comparable to that in Christiansen et al.[21,23], which uses a finer grid resolution.

To represent the deceleration of flow due to monopile-induced drag, the drag parameterization is incorporated into the hydrostatic momentum equation given by

$$\frac{D\vec{u}}{Dt} = \frac{\partial}{\partial z}\left(\nu \frac{\partial \vec{u}}{\partial z}\right) - g\nabla\eta + \vec{F} + \vec{G}_d, \tag{4}$$

where ν is the vertical eddy viscosity, g is gravitational acceleration, η is the free-surface elevation, and $\vec{F}$ represents additional forcing terms, such as baroclinic gradient, horizontal viscosity and the Coriolis force[47].

To further account for the generation of subgrid-scale wake turbulence, the drag term $\vec{G}_d$ is also included in the turbulence closure scheme governing the evolution of TKE k and its dissipation rate ϵ, using the generic length-scale model[57,60,61]. Here, subgrid-scale wake turbulence denotes turbulence generated by individual monopile wakes that occur at spatial scales smaller than the model grid resolution and is therefore parameterized rather than explicitly resolved[23]. The modified governing equations are given by

$$\frac{\partial k}{\partial t} = \frac{\partial}{\partial z}\left(\nu_k \frac{\partial k}{\partial z}\right) + P + B - \epsilon - \left(\vec{G}_d \cdot \vec{u}\right), \tag{5}$$

$$\frac{\partial \epsilon}{\partial t} = \frac{\partial}{\partial z}\left(\nu_\epsilon \frac{\partial \epsilon}{\partial z}\right) + \frac{\epsilon}{k}\left(c_1 P + c_3 B - c_2 \epsilon F_{wall} - c_4\left(\vec{G}_d \cdot \vec{u}\right)\right), \tag{6}$$

where ν_k and ν_ϵ are the vertical turbulent diffusivities for k and ϵ, respectively. F_{wall} is a wall-proximity function, P and B represent shear and buoyancy production, respectively, and c_1, c_2, c_3, c_4 are model-specific empirical coefficients associated with source and sink terms in the dissipation equation[62]. In the implementation of the k-ϵ turbulence model, we adopted the standard values of $c_1 = 1.44$, $c_2 = 1.92$ and $c_3 = -0.52$. The coefficient c_4, which modulates the contribution of wake-generated turbulence to dissipation, is more physically sensitive and less universally defined. While Rivier et al.[61] adopted $c_4 = c_2$, Rennau et al.[57] emphasized the physical implications of varying c_4, showing that mixing efficiency increases for $c_4 < c_1$ and decrease for $c_4 > c_1$. Based on their findings, which suggest an upper bound of $c_4 = 1.75$, and their proposed values of $c_4 = 0.6$ for strong mixing and $c_4 = 1.4$ for weak mixing regimes, we set $c_4 = 1.0$ in this study to reflect a moderate mixing scenario. All offshore windfarm parameters are summarized in Table 2.

Table 2 | Parameter value and reference sources for offshore windfarm parameterization

Parameter	Value	Reference source/Note
Maximum wind speed deficit, a	10%	Supplementary Table 2
Wake decay length, σ	30 km	Supplementary Table 2
Turbine drag coefficient, C_d	1	Shih et al.[58]; Sumer[59]; Carpenter et al.[16]; Christiansen et al.[21,23]
Monopile diameter, d	8 m	4C Offshore

Offshore wind farms distribution and numerical experiments

Wind farm extents and turbine densities were derived from the 4C Offshore dataset. In this study, we applied the OWF configurations representing present-day (operating) scenarios. To assess the influence of OWFs on hydrodynamics and sediment dynamics, we conducted simulations with and without OWF effects, allowing comparison between wake-affected and reference conditions.

A total of 15 model experiments (Table 3) were conducted to assess model uncertainty related to variation of two key parameters, namely particle settling velocity (w_s) and critical shear stress for resuspension (τ_c). The reference simulations (e.g., S1_REF) exclude any OWF effect, while the simulations with OWFs (e.g., S1_OWF) incorporate effects in both atmospheric and oceanic compartments. To distinguish OWF-induced impacts from natural variability, differences between the simulations with OWF effects and corresponding reference simulations adopting the same setting of w_s and τ_c were calculated (e.g., S1_OWF – S1_REF).

To distinguish the effects between atmospheric wakes and oceanic wakes, one additional experiment was conducted. This experiment (S1_OWF_noturb) considers effect of OWF-induced wind changes but excludes effects of OWF-induced hydrodynamic drag and turbulence in water. A comparison between this experiment and the one with OWF effects in both atmosphere and ocean (S1_OWF) helps to distinguish the effects of OWF-induced changes in the two compartments in driving large-scale sediment transport. Results indicate that the changes of TKE in ocean caused by wind turbines are mainly confined inside the OWFs (Supplementary Fig. 5).

Sediment transport steadiness analysis

As a measure of directional stability of residual sediment transport flux, we computed the ratio of vector mean to scalar mean fluxes from the numerical model output as

$$S = \frac{\sqrt{\bar{Q}_{s,x}^{\,2} + \bar{Q}_{s,y}^{\,2}}}{\left|\bar{Q}_s\right|} \in [0,\ 1], \tag{7}$$

where $Q_{s,x}$ and $Q_{s,y}$ are the east-west and north-south components of the residual sediment transport flux vector Q_s, respectively, and an overbar denotes temporal averages. This parameter was initially proposed by Ramster et al.[63] as a measure of current steadiness and has also been used in morphodynamic studies measuring steadiness of sediment transport direction[64,65]. Values close to unity denote high directional residual sediment flux stability, whereas values close to zero denote essentially random flux directions.

Table 3 | Summary of numerical experiments for this study

		w_s (mm/s)				τ_c (Pa)			
		POC	Silt	Very fine sand	River ine silt	POC	Silt	Very fine sand	River ine silt
S1_REF	Reference simulation S1	0.05	0.05	1.0	0.05	0.2	0.2	1.0	0.2
S1_OWF	Simulation S1 with OWFs effect in both atmosphere and ocean								
S1_OWF_noturb	Simulation S1 with OWFs effect only in atmosphere								
S2_REF	Reference simulation S2	0.05	0.05	1.0	0.05	0.05	0.05	1.0	0.05
S2_OWF	Simulation S2 with OWFs effect in both atmosphere and ocean								
S3_REF	Reference simulation S3	0.2	0.2	1.0	0.2	0.05	0.05	1.0	0.05
S3_OWF	Simulation S2 with OWFs effect in both atmosphere and ocean								
S4_REF	Reference simulation S4	0.2	0.2	1.0	0.2	0.1	0.1	1.0	0.1
S4_OWF	Simulation S4 with OWFs effect in both atmosphere and ocean								
S5_REF	Reference simulation S5	0.1	0.1	1.0	0.1	0.1	0.1	1.0	0.1
S5_OWF	Simulation S5 with OWFs effect in both atmosphere and ocean								
S6_REF	Reference simulation S6	0.01	0.01	1.0	0.01	0.05	0.05	1.0	0.05
S6_OWF	Simulation S6 with OWFs effect in both atmosphere and ocean								
S7_REF	Reference simulation S7	0.4	0.4	1.0	0.4	0.2	0.2	1.0	0.2
S7_OWF	Simulation S7 with OWFs effect in both atmosphere and ocean								

Indicator for stratification

Potential energy anomaly (PEA) quantifies the strength of water-column stratification and represents the amount of energy required to fully mix the water column to uniform density[66]. Higher PEA values indicate stronger stratification. It is calculated from the vertical density distribution as

$$\varphi = \int_{-h}^{0} (\rho - \langle\rho\rangle) g z dz, \tag{8}$$

$$\langle\rho\rangle = \frac{1}{h}\int_{-h}^{0} \rho dz, \tag{9}$$

where h is the depth of the water column, ρ and $<\rho>$ the vertical density profile over the water column and the depth-averaged density, z the vertical coordinate and g the gravitational acceleration.

Data availability

Previously published datasets used in this study are cited in Methods with details listed in Supplementary Table 1.

Code availability

The source codes of SCHISM are available from the DOI 10.5281/zenodo.6537526 and is licensed under open-source Apache license version 2[47]. Figures were made with matlab R2024b-gcc-13.3.0 through the German Climate Computing Centre (DKRZ) platform. The numerical modeling result and the matlab scripts for visualization are available from DOI 10.5281/zenodo.18714062.

Received: 29 September 2025; Accepted: 2 March 2026;
Published online: 14 March 2026

References

1. IEA. Renewables 2024, IEA, Paris. https://www.iea.org/reports/renewables-2024 (2024).
2. WindEurope. Wind energy in Europe: 2024 Statistics and the outlook for 2025–2030. https://windeurope.org/intelligence-platform/product/wind-energy-in-europe-2024-statistics-and-the-outlook-for-2025-2030/ (2024).
3. Hanebuth, T. J., Lantzsch, H. & Nizou, J. Mud depocenters on continental shelves—appearance, initiation times, and growth dynamics. *Geo Mar. Lett.* **35**, 487–503 (2015).
4. Zhang, W. et al. Long-term carbon storage in shelf sea sediments reduced by intensive bottom trawling. *Nat. Geosci.* **17**, 1268–1276 (2024).
5. Zhang, W. et al. Quantifying importance of macrobenthos for benthic-pelagic coupling in a temperate coastal shelf sea. *J. Geophys. Res.* **126**, e2020JC016995 (2021).
6. Vanhellemont, Q. & Ruddick, K. Turbid wakes associated with offshore wind turbines observed with Landsat 8. *Remote Sens. Environ.* **145**, 105–115 (2014).
7. Li, X., Chi, L., Chen, X., Ren, Y. & Lehner, S. SAR observation and numerical modeling of tidal current wakes at the East China Sea offshore wind farm. *J. Geophys. Res.* **119**, 4958–4971 (2014).
8. Baeye, M. & Fettweis, M. In situ observations of suspended particulate matter plumes at an offshore wind farm, southern North Sea. *Geo Mar. Lett.* **35**, 247–255 (2015).
9. Akhtar, N., Geyer, B., Rockel, B., Sommer, P. S. & Schrum, C. Accelerating deployment of offshore wind energy alter wind climate and reduce future power generation potentials. *Sci. Rep.* **11**, 1–12 (2021).
10. Djath, B., Johannes S.-S. & Beatriz, C. Impact of atmospheric stability on X-band and C-band synthetic aperture radar imagery of offshore windpark wakes. *J. Renew. Sustain. Energy* **10**, 043301 (2018).
11. Cañadillas, B. et al. Offshore wind farm wake recovery: Airborne measurements and its representation in engineering models. *Wind Energy* **23**, 1249–1265 (2020).
12. Platis, A. et al. Long-range modifications of the wind field by offshore wind parks–results of the project WIPAFF. *Meteorol. Z.* **29**, 355–376 (2020).
13. Ludewig, E. *Influence of Offshore Wind Farms on Atmosphere and Ocean Dynamics* (University of Hamburg, 2014).
14. Broström, G. On the influence of large wind farms on the upper ocean circulation. *J. Mar. Syst.* **74**, 585–591 (2008).
15. Floeter, J., Pohlmann, T., Harmer, A. & Möllmann, C. Chasing the offshore wind farm wind-wake-induced upwelling/downwelling dipole. *Front. Marine Sci*. **9**, 16 (2022).
16. Carpenter, J. R. et al. Potential impacts of offshore wind farms on North Sea stratification. *PloS one* **11**, e0160830 (2016).
17. van Berkel, J. et al. The effects of offshore wind farms on hydrodynamics and implications for fishes. *Oceanography* **33**, 108–117 (2020).
18. Hendriks, E. et al. The impact of offshore wind turbine foundations on local hydrodynamics and stratification in the Southern North Sea. *Front. Mar. Sci.* **12**, 1619577 (2025).
19. Forster, R. M. The effect of monopile-induced turbulence on local suspended sediment pattern around UK wind farms. An IECS report to The Crown Estate https://ore.catapult.org.uk/wp-content/uploads/2018/12/The-Effect-of-Monopile-Induced-Turbulence-on-Local-Suspended-Sediment-Pattern-around-UK-Wind-Farms.pdf (2018).
20. Christiansen, N., Daewel, U., Djath, B. & Schrum, C. Emergence of large-scale hydrodynamic structures due to atmospheric offshore wind farm wakes. *Front. Mar. Sci.* **9**, 818501 (2022).
21. Christiansen, N., Daewel, U. & Schrum, C. Cumulative hydrodynamic impacts of offshore wind farms on North Sea currents and surface temperatures. *Commun. Earth Environ.* **7**, 164 (2026).
22. Daewel, U., Akhtar, N., Christiansen, N. & Schrum, C. Offshore wind farms are projected to impact primary production and bottom water deoxygenation in the North Sea. *Commun. Earth Environ.* **3**, 292 (2022).
23. Christiansen, N., Carpenter, J. R., Daewel, U., Suzuki, N. & Schrum, C. The large-scale impact of anthropogenic mixing by offshore wind turbine foundations in the shallow North Sea. *Front. Mar. Sci.* **10**, 1178330 (2023).
24. Mayer, L. M. Surface area control of organic carbon accumulation in continental shelf sediments. *Geochim. Cosmochim. Acta* **58**, 1271–1284 (1994).
25. Christiansen, N., Daewel, U. & Schrum, C. Tidal mitigation of offshore wind wake effects in coastal seas. *Front. Mar. Sci.* **9**, 1006647 (2022).
26. Chen, J. et al. Physical mechanisms of sediment trapping and deposition on a spatially confined mud depocenter in a high-energy shelf sea. *J. Geophys. Res.* **130**, e2025JC022622 (2025).
27. Eisma, D. Supply and deposition of suspended matter in the North Sea. In *Holocene Marine Sedimentation in the North Sea Basin*, (eds Nio, S.-.-D., Shüttenhelm, R.T.E. & Van Weering, T.C.E.) 415–428 https://doi.org/10.1002/9781444303759.ch29 (1981).
28. Porz, L. et al. Quantification and mitigation of bottom-trawling impacts on sedimentary organic carbon stocks in the North Sea. *Biogeosciences* **21**, 2547–2570 (2024).
29. de Haas, H., van Weering, T. C. & de Stigter, H. Organic carbon in shelf seas: sinks or sources, processes and products. *Cont. Shelf Res.* **22**, 691–717 (2002).
30. Diesing, M., Thorsnes, T. & Bjarnadóttir, L. R. Organic carbon densities and accumulation rates in surface sediments of the North Sea and Skagerrak. *Biogeosciences* **18**, 2139–2160 (2021).
31. Wolf, J. The estimation of shear stresses from near-bed turbulent velocities for combined wave–current flows. *Coast. Eng.* **37**, 529–543 (1999).

32. Winterwerp, J. C., Van Kesteren, W. G. M., Van Prooijen, B. & Jacobs, W. (2012). A conceptual framework for shear flow–induced erosion of soft cohesive sediment beds. *J. Geophys. Res. Oceans*, 117 (2012).
33. Geyer, W. R., Hill, P. S. & Kineke, G. C. The transport, transformation and dispersal of sediment by buoyant coastal flows. *Continental Shelf Res.* **24**, https://doi.org/10.1016/j.csr.2004.02.006 (2004).
34. Castaing, P. et al. Relationship between hydrology and seasonal distribution of suspended sediments on the continental shelf of the Bay of Biscay. *Deep Sea Res. Part II* **46**, https://doi.org/10.1016/S0967-0645(99)00052-1 (1999).
35. Liu, J. T. et al. A comprehensive sediment dynamics study of a major mud belt system on the inner shelf along an energetic coast. *Sci. Rep.* **8**, https://doi.org/10.1038/s41598-018-22696-w (2018).
36. Kämpf, J. Extreme bed shear stress during coastal downwelling. *Ocean Dyn.* **5**, 69 (2019).
37. Zhang, W., Cui, Y., Santos, A. I. & Hanebuth, T. J. J. Storm-driven bottom sediment transport on a high-energy narrow shelf (NW Iberia) and development of mud depocenters. *J. Geophys. Res. Oceans* **121**, https://doi.org/10.1002/2015JC011526 (2016).
38. Ricker, M., Meyerjürgens, J., Badewien, T. H. & Stanev, E. V. (2021). Lagrangian methods for visualizing and assessing frontal dynamics of floating marine litter with a focus on tidal basins. In *Chemical Oceanography of Frontal Zones*, (eds Belkin, I. M.) **116**, 407–442 (Springer, Berlin, Heidelberg, 2021). https://doi.org/10.1007/698_2021_812
39. Porz, L. et al. Dredging and dumping impact coastal fluxes of sediment and organic carbon. *Nat. Commun.* **17**, 216 (2026).
40. Miao, B., Arlinghaus, P., Ho-Hagemann, H. T. M., Schrum, C. & Zhang, W. Misconception of coastal morphological resilience caused by inconsistent resolution in bathymetry mapping. *Commun. Earth Environ.* **6**, 904 (2025).
41. Xu, G., Bi, S., Gugliotta, M., Liu, J. & Liu, J. P. Dispersal mechanism of fine-grained sediment in the modern mud belt of the East China Sea. *Earth Sci. Rev.* **240**, 104388 (2023).
42. Ivanov, E. et al. Offshore wind farm footprint on organic and mineral particle flux to the bottom. *Front. Mar. Sci.* **8**, 631799 (2021).
43. De Borger, E. et al. Offshore windfarm footprint of sediment organic matter mineralization processes. *Front. Mar. Sci.* **8**, 632243 (2021).
44. Heinatz, K. & Scheffold, M. I. E. A first estimate of the effect of offshore wind farms on sedimentary organic carbon stocks in the Southern North Sea. *Front. Mar. Sci.* **9**, 1068967 (2023).
45. Grashorn, S. & Stanev, E. V. Kármán vortex and turbulent wake generation by wind park piles. *Ocean Dyn.* **66**, 1543–1557 (2016).
46. Hosseini, S. T., Pein, J., Staneva, J., Zhang, Y. J. & Stanev, E. Impact of offshore wind farm monopiles on hydrodynamics interacting with wind-driven waves. *Ocean Model.* **195**, 102521 (2025).
47. Zhang, Y. J., Ye, F., Stanev, E. V. & Grashorn, S. Seamless cross-scale modeling with SCHISM. *Ocean Model.* **102**, 64–81 (2016).
48. Pinto, L., Fortunato, A., Zhang, Y., Oliveira, A. & Sancho, F. Development and validation of a three-dimensional morphodynamic modelling system for non-cohesive sediments. *Ocean Model.* **57**, 1–14 (2012).
49. Roland, A. *Development of WWM II: Spectral Wave Modelling on Unstructured Meshes*. Doctoral dissertation, Ph. D. thesis (Technische Universität Darmstadt, Institute of Hydraulic and Water Resources Engineering, 2008).
50. Kossack, J., Mathis, M., Daewel, U., Zhang, Y. J. & Schrum, C. Barotropic and baroclinic tides increase primary production on the Northwest European Shelf. *Front. Mar. Sci.* **10**, 1206062 (2023).
51. Chelton, D. B., Deszoeke, R. A., Schlax, M. G., el Naggar, K. & Siwertz, N. Geographical variability of the first baroclinic Rossby radius of deformation. *J. Phys. Oceanogr.* **28**, 433–460 (1998).
52. Bockelmann, F.-D., Puls, W., Kleeberg, U., Müller, D. & Emeis, K.-C. Mapping mud content and median grain-size of North Sea sediments–a geostatistical approach. *Mar. Geol.* **397**, 60–71 (2018).
53. Sievers, J., Malte, R., Milbradt, P. EasyGSH-DB: Subject area - Sedimentology [Data set]. https://doi.org/10.48437/02.2020.K2.7000.0005 (2020).
54. Colina Alonso, A. et al. A mud budget of the Wadden Sea and its implications for sediment management. *Commun. Earth Environ.* **5**, 153 (2024).
55. Heyer, H. & Schrottke, K. Aufbau von integrierten Modellsystemen zur Analyse der langfristigen Morphodynamik in der Deutschen Bucht: AufMod; gemeinsamer Abschlussbericht für das Gesamtprojekt mit Beiträgen aus allen 7 Teilprojekten. Bundesamt für Seeschifffahrt und Hydrographie (BSH) (2013).
56. Abril, G. et al. Behaviour of organic carbon in nine contrasting European estuaries. *Estuar. Coast. Shelf Sci.* **54**, 241–262 (2002).
57. Rennau, H., Schimmels, S. & Burchard, H. On the effect of structure-induced resistance and mixing on inflows into the Baltic Sea: a numerical model study. *Coast. Eng.* **60**, 53–68 (2012).
58. Shih, W. C. L., Wang, C., Coles, D. & Roshko, A. Experiments on flow past rough circular cylinders at large Reynolds numbers. *J. Wind Eng. Ind. Aerodyn.* **49**, 351–368 (1993).
59. Sumer, B. M. *Hydrodynamics Around Cylindrical Strucures*, Vol. 26. (World scientific, 2006).
60. Svensson, U. & Häggkvist, K. A two-equation turbulence model for canopy flows. *J. Wind Eng. Ind. Aerodyn.* **35**, 201–211 (1990).
61. Rivier, A., Bennis, A.-C., Pinon, G., Magar, V. & Gross, M. Parameterization of wind turbine impacts on hydrodynamics and sediment transport. *Ocean Dyn.* **66**, 1285–1299 (2016).
62. Umlauf, L. & Burchard, H. A generic length-scale equation for geophysical turbulence models. *J. Mar. Res.* **61**, 235–265 (2003).
63. Ramster, J. W., Hughes, D. G. & Furnes, G. K. A 'steadiness' factor for estimating the variability of residual drift in current meter records. *Dtsch. Hydrografische Z.* **31**, 230–236 (1978).
64. Poulos, S. The contribution of near-bed currents to modern sedimentation processes in the deep waters of the Hellenic Arc-Trench system, eastern Mediterranean. *Geo Mar. Lett.* **20**, 201–208 (2001).
65. Porz, L., Zhang, W. & Schrum, C. Natural and anthropogenic influences on the development of mud depocenters in the southwestern Baltic Sea. *Oceanologia* **65**, 182–193 (2023).
66. Simpson, J. H., Allen, C. M. & Morris, N. C. G. Fronts on the continental shelf. *J. Geophys. Res. Oceans* **83**, 4607–4614 (1978).

Acknowledgements

This study is a contribution to the CoastalFutures-2 project (03F0980A) in the DAM research mission and the MARE:N project "Anthropogenic impacts on particulate organic carbon cycling in the North Sea (APOC)" (03F0874C) both funded by BMFTR. It is also supported by the Helmholtz research programme POF IV "The Changing Earth – Sustaining our Future" on "Topic 4: Coastal zones at a time of global change". L.P. is supported by the collaborative project KomSO (grant 3523NK370A-E) coordinated by the German Federal Agency for Nature Conservation (BfN). This work used resources of the German Climate Computing Centre (DKRZ) granted by its Scientific Steering Committee (WLA) under project ID bg1244, gg1302 and bg1315.

Author contributions

Jiayue Chen: Writing – original draft, Software, Methodology, Visualization. Nils Christiansen: Software, Resources, Methodology, Data curation, Formal analysis, Writing – review & editing. Lucas Porz: Software, Methodology, Formal analysis, Writing – review & editing. Bo Miao: Software, Visualization. Mengyao Ma: Software. Corinna Schrum: Supervision, Project administration, Writing – review & editing. Wenyan Zhang: Writing – review & editing, Supervision, Project administration, Methodology, Formal analysis.

Funding

Open Access funding enabled and organized by Projekt DEAL.

Competing interests
The authors declare no competing interests.

Additional information
Supplementary information The online version contains supplementary material available at https://doi.org/10.1038/s43247-026-03390-6.

Correspondence and requests for materials should be addressed to Wenyan Zhang.

Peer review information *Communications Earth and Environment* thanks Emil De Borger and the other, anonymous, reviewer(s) for their contribution to the peer review of this work. Primary Handling Editors: Yang Yang, Alice Drinkwater and Nandita Basu. A peer review file is available.